Fall 2018

Smart augmented reality instructional system for mechanical assembly

Ze-Hao Lai

SMART AUGMENTED REALITY INSTRUCTIONAL SYSTEM

FOR MECHANICAL ASSEMBLY

by

ZE-HAO LAI

A THESIS

Presented to the Faculty of the Graduate School of the

MISSOURI UNIVERSITY OF SCIENCE AND TECHNOLOGY

In Partial Fulfillment of the Requirements for the Degree

MASTER OF SCIENCE IN MANUFACTURING ENGINEERING

2018

Approved by:

Ming C. Leu, Advisor

Zhaozheng Yin

Ruwen Qin

ABSTRACT

Quality and efficiency are pivotal indicators of a manufacturing company. Many companies are suffering from shortage of experienced workers across the production line to perform complex assembly tasks such as assembly of an aircraft engine. This could lead to a significant financial loss. In order to further reduce time and error in an assembly**,** a smart system consisting of multi-modal Augmented Reality (AR) instructions with the support of a deep learning network for tool detection is introduced. The multi-modal smart AR is designed to provide on-site information including various visual renderings with a fine-tuned Region-based Convolutional Neural Network, which is trained on a synthetic tool dataset. The dataset is generated using CAD models of tools augmented onto a 2D scene without the need of manually preparing real tool images. By implementing the system to mechanical assembly of a CNC carving machine, the result has shown that the system is not only able to correctly classify and localize the physical tools but also enables workers to successfully complete the given assembly tasks. With the proposed approaches, an efficiently customizable smart AR instructional system capable of sensing, characterizing the requirements, and enhancing worker's performance effectively has been built and demonstrated.

ACKNOWLEDGMENTS

I would like to express my greatest gratitude to my advisor, Dr. Ming C. Leu, for his support and guidance in every aspect throughout my graduate study. I would like to thank my committee members, Dr. Yin and Dr. Qin, for all the research advice regarding machine learning and engineering system.

I would like to acknowledge and thank all the funding sources granted from National Science Foundation CMMI-1646162 and the Intelligent Systems Center at Missouri University of Science and Technology.

Furthermore, I would like to thank Dr. Randy Moss for helping me in exploring the field of machine vision, and my previous colleagues in Aerospace Industrial Development Corporation for providing practical insights from the industry.

Finally, I would like to thank my family for always being supportive along the way of my study. In addition, I would like to thank Wenjin Tao for his help of the work and valuable suggestions. I would also like to thank Md. Moniruzzaman, Chia-Hung Hung, Viraj Gajjar, Whamsy Kryshna, and all the members of Innovative Additive Manufacturing lab for all the support.

TABLE OF CONTENTS

Page

ABSTRACT iii

ACKNOWLEDGMENTS iv

LIST OF ILLUSTRATIONS vii

LIST OF TABLES ix

SECTION

1. INTRODUCTION 1

 1.1. BACKGROUND AND MOTIVATION 1

 1.2. RELATED WORK 3

 1.3.OVERVIEW OF THE PROPOSED SYSTEM 5

2. TECHNOLOGY COMPONENTS AND SYSTEM OVERVIEW 6

 2.1. MULTI-MODAL AUGMENTED REALITY 6

  2.1.1. Feature Extraction 7

  2.1.2. Camera Pose Estimation for Augmented Reality 8

  2.1.3. Multi-modal AR Realization 11

 2.2. DEEP LEARNING FOR TOOL DETECTION 13

  2.2.1. Detection Approach 13

  2.2.2. Synthetic Dataset 14

  2.2.3. Faster R-CNN 17

 2.3. SYSTEM OVERVIEW 21

3. EXPERIMENT 23

3.1. EXPERIMENTAL SETUP 23
3.2. SYSTEM EVALUATION 26
3.2.1. Subject Selection and Testing Procedure 26
3.2.2. Evaluation Metric 27
4. RESULTS 29
4.1. TOOL DETECTOR AND SMART AR RENDERING 30
4.2. SYSTEM EVALUATION AND DISCUSSION 34
5. CONCLUSION 41
APPENDIX 42
BIBLIOGRAPHY 48
VITA 52

LIST OF ILLUSTRATIONS

Figure Page

1.1. Highly complex assembly of an aircraft engine 1

1.2. Overview of the proposed system.. 5

2.1. The proposed multi-modal AR instructional system 6

2.2. A selected image for the target marker 7

2.3. The detected features (corners) on the marker... 8

2.4. The pipeline of realizing AR.. 9

2.5. The homography transformation between the two coordinate systems.................... 10

2.6. An example frame of an AR effect 11

2.7. An example frame of multi-modal AR for a mechanical assembly.......................... 12

2.8. The system workflow of deep learning supported AR for tooling in assembly 13

2.9. Synthetic dataset for R-CNN pipeline 14

2.10. Synthetic data: 5 classes of CAD models of the synthetic tool dataset 15

2.11. A synthetic tool rotates about three different axes... 16

2.12. Synthetic data for R-CNN... 17

2.13. Region proposal network (RPN)... 18

2.14. Faster R-CNN architecture 18

2.15. The workflow of the integrated system 21

2.16. The derived transformation matrix maps the coordinate to a video frame of AR .. 22

3.1. A workstation setup for the experiment... 23

3.2. The z-axis mechanism of the spindle assembly... 24

3.3. The installed spindle with the z-axis 24

3.4. The Intersection over Union (IoU) 28

4.1. A subject is performing the experiment using the paper manual 29

4.2. A subject is performing the experiment using the Smart AR system 29

4.3. Tool detection using Faster R-CNN with a surveillance camera 30

4.4. The results of detecting real tools with various orientations 31

4.5. Example frames of False Positive (FP) 33

4.6. AR integrated with the tool detector for Step 3 of the assembly task 33

4.7. AR integrated with the tool detector for Step 4 of the assembly task 34

4.8. The mean completion time of two groups 36

4.9. The mean number of errors of two groups 36

4.10. The comparison of three types of error 37

4.11. Two subjects perform Step 2 with two different instructional guidance 39

4.12. The wear of a V-wheel mechanism caused by the installation error 39

LIST OF TABLES

Table Page

3.1. The spindle assembly task 25

3.2. Three types of assembly errors 27

4.1. Average Precision on detecting different real tools.. 32

4.2. Results of the group using paper manual.. 34

4.3. Results of the group using smart AR instructional system....................................... 35

4.4. Percentage reduction for each type of errors using the AR instruction 37

4.5. Error analysis of the experiment with the paper manual 38

4.6. Error analysis of the experiment with the smart AR system 38

1. INTRODUCTION

1.1. BACKGROUND AND MOTIVATION

In the Industry 4.0 era, consumer needs towards products of high quality, high complexity and mass customization have been growing in a fast-moving pace. Many companies are seeking solutions that could increase the efficacy. However, the state of having shortage of experienced workforce has always been a critical problem while employers are facing the rapid transition of industry. According to a Honeywell news [1], 78% of the modern technology is considered important, 65% of the technological advances are restrained by the outdated work styles, and 38% of the current workers are actively looking for a different position. That has reflected the urgent needs for the system update and flexibility for workforce training. Also, the quality of products plays a vital role as the difficulty of assembly increases, e.g., a jet engine is comprised of more than 10,000 individual parts. Figure 1.1. shows the photo of an aircraft engine assembly that contains a wide variety of machine parts.

Figure 1.1. Highly complex assembly of an aircraft engine [2]

As reported by GE [3], the company loses millions of dollars each year because nuts and hoses that seal fluid lines are not fastened right for the jet engine, which leads to an unnecessary cost from repairing, not to mention the safety of passengers. Therefore, to improve the productivity, the ability to sense, monitor, characterize, and support the workers for highly complex assembly has become even more imperative, especially when conducting unpleasant, unsafe, exhausting tasks. To remain competitive, companies and researchers have been attempting for solutions toward smart manufacturing by applying emerging technologies such as Artificial Intelligence (AI), Internet-of-Things (IoT) and industrial digital twin [4]. Many leading manufacturing companies have already noticed the potential and started piloting Virtual Reality (VR) and Augmented Reality (AR) technologies, which has been successfully utilized in various fields ranging from medical area [5], to the assembly line. The significant reduction of errors, time, and training requirements have been measured and proven by the Augmented Reality for Enterprise Alliance (AREA) of Boeing. "This has tremendous potential to minimize errors, cut down on costs and improve product quality" [3]. GE has witnessed the improvement in productivity and efficiency by implementing AR. Honeywell also proved the success in worker training with the usage of AR [1].

Although AR rendering for assembly has been demonstrated for its promising potential, industries still do not have real-world solutions aiming at further increasing the productivity by minimizing the assembly time and error with the assistance of AR. There are five challenges that need to be addressed as follows:

1. The commercialized AR supported devices are usually too heavy to wear and too expensive. This may cause concerns for practical industry use of AR devices,

especially at the assembly line. The accessibility and usability of the selected resources for system development is important.

2. Besides the potential of implementing AR in the assembly industry, how an AR guiding system need to be further improved to assist workers.
3. The capability of onsite multi-modal AR instructions needs to be provided to enhance the knowledge transfer.
4. The capability of sensing, tracking and characterizing a working environment needs to be advanced to provide natural, interactive feedback while workers are performing an assembly.
5. The high flexibility and efficiency of system update in terms of data acquisition are imperative, which are the essentials for Internet of Things (IoT) in smart manufacturing.

1.2. RELATED WORK

In the scientific perspective, many researchers have emphasized the benefits that AR could bring to the industry. Tao et al. [6] discussed the state-of-the-art VR/AR technologies for assembly simulations including modeling, sensing, and interaction. Caudell et al. [7] proposed an AR application for manual manufacturing processes. Azuma et al. [8] presented the potential of AR with head-mounted display (HMD). Over the past decade, more and more research regarding engineering assembly has become popular as engineers have applied AR to different engineering scenarios [9-13]. For AR training, Webel et al. [14] raised the problem of handheld device during assembly. Leu et al. [15] pointed out research efforts needed to improve the realism of virtual assembly, such as high-fidelity dynamic graphic displays, low-cost sensor fusion techniques, haptic devices, and multi-modal rendering such as audio rendering [16]. Also, the lack of natural, interactive mechanisms between the assembly operators, the assembly of components, and the instructions being rendered need to be addressed. Werrlich et al. [17, 18] presented an overview of evaluations using AR training, identifying the current limitations pertaining to high similarities of existing designed experiments that need to be improved.

With the advancement of technologies in machine learning, machines are now able to recognize and classify objects and activities by using different classification methods [19, 20]. Davide et al. [21, 22] successfully recognized basic motions using signals captured from a smartphone by extracting features using classification. Ward et al. [23] proposed a strategy for recognizing assembly motions. Tao et al. [24] developed a Convolutional Neural Networks (CNN) model to recognize the worker activity using IMU and sEMG signals captured from an armband. Al-Amin et al. [25] used a Kinect sensor to perceive the worker's activity for workforce modeling and management. Overall, the number of research papers regarding deep learning [26] methods, such as pattern recognition using CNN [27], R-CNN [28, 29] for object detection, have been growing rapidly. In addition, the research pertaining to learning features from synthetic dataset using data augmentation was presented [30, 31] for 3D object and pedestrian detection, which identifies the utility when training data is limited.

1.3. OVERVIEW OF THE PROPOSED SYSTEM

A smart AR instructional system with the support of deep learning is introduced in this study, which is intended to further improve the performance of a worker through assistive smart instruction. To develop the system, a combination of sensors is applied to capture the information of a working area while the augmented view is rendered via an onsite display. Once the environmental data has been obtained, the captured information are sent to a fine-tuned deep learning model for decision making. After that, the predicted results are transmitted to the AR system through an Internet Protocol (IP) as the system will superimpose AR information accordingly in a worker's view for assembly instruction rendering. Figure 1.2 summarizes the overall system workflow.

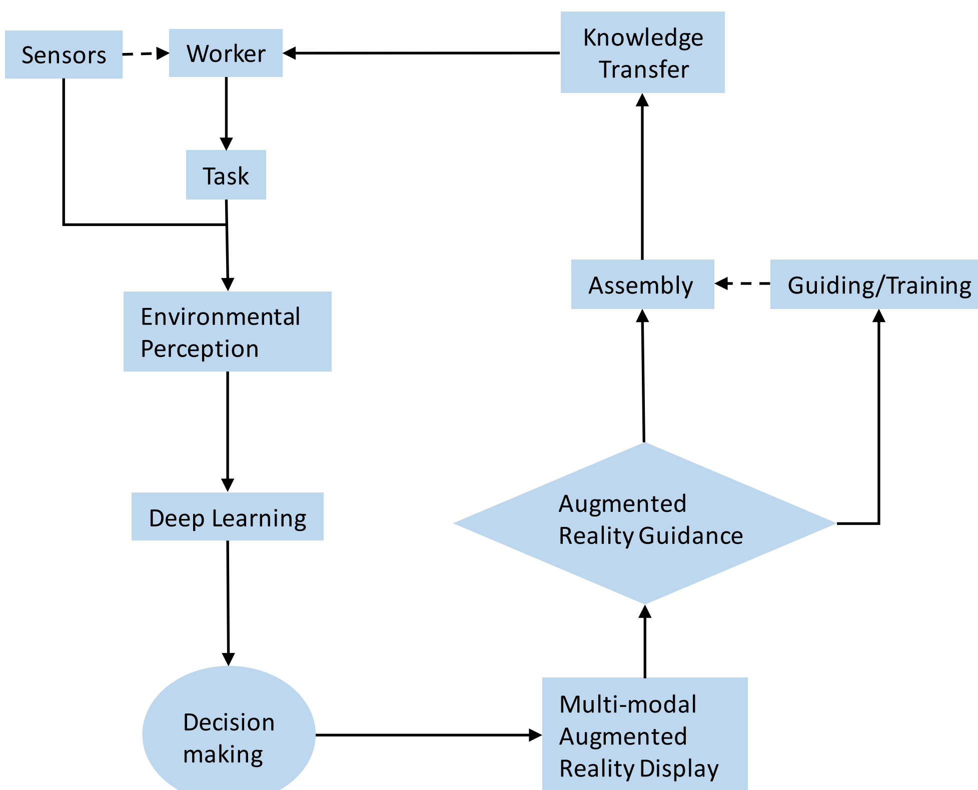

Figure 1.2. Overview of the proposed system

2. TECHNOLOGY COMPONENTS AND SYSTEM OVERVIEW

2.1. MULTI-MODAL AUGMENTED REALITY

To visualize and understand onsite instructions, an AR instructional system which offers multi-threading display including texts, graphics, animations by applying data fusion needs to be created. With multi-modal AR instructions, workers are able to directly sense and comprehend the physical environment while following the AR instructions step by step. Figure 2.1. illustrates the proposed multi-modal AR system.

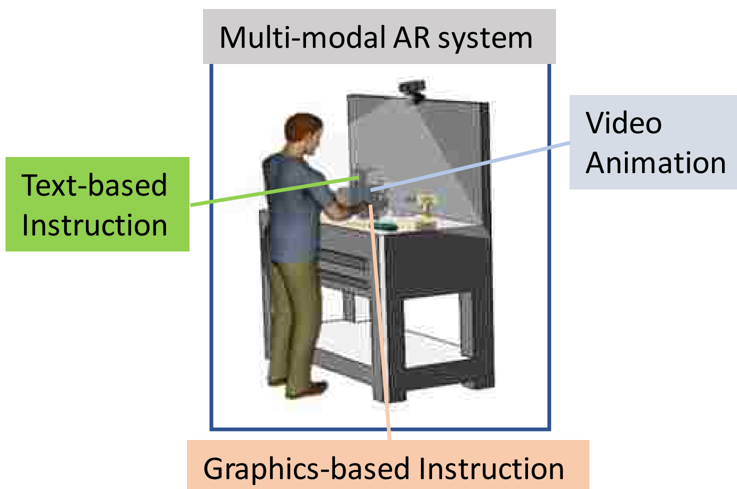

Figure 2.1. The proposed multi-modal AR instructional system

To realize the multi-modal AR display, a marker is attached to a workbench so the webcam can perceive the information of the patterns from the marker for feature recognition and tracking, so as to superimpose the computer-generated (CG) data in a worker's view. To successfully achieve the data overlaying process, an effective camera pose estimation approach for coordinate transformation is required. The process of achieving multi-modal AR involves several technology components as described in the following sections.

2.1.1. Feature Extraction. Features (corners) are first to be extracted for target recognition. Corners are regions within the image with large variations in intensity, which can be detected using a sliding window to measure intensity change. The equation of the sliding window is:

$$E(u,v) = \sum_{x,y} w(x,y)[I(x+u,y+v) - I(x,y)]^2 \tag{1}$$

where $w(x,y)$ is the window function on the position of x and y within an image. $I(x,y)$ is the gradient at (x,y). u and v are represented as the shifting distances in x and y directions, respectively. To find the features (corners) that yield the highest $E(u,v)$, the second term needs to be maximized, meaning the largest change in intensity $E(u,v)$. Figure 2.2 presents a selected image for the target marker in this study due to its large number of features (corners).

Figure 2.2. A selected image for the target marker

Figure 2.3 illustrates the corners on the marker which are detected as features for target recognition and tracking, which can be utilized for developing a 3D world coordinate system based on the target marker for camera pose estimation.

Figure 2.3. The detected features (corners) on the marker. Corners represent the regions which have the highest change in intensity in all directions, which are highlighted with yellow '+'.

2.1.2. Camera Pose Estimation for Augmented Reality. After finishing extracting features from a single frame, the estimation for camera pose using homography transformation begins in order to realize AR effect. Figure 2.4. illustrates the pipeline of realizing AR. To augment a computer-generated data onto a scene, a homography transformation is applied to estimate the camera pose for overlaying data spatially using a projection matrix. In this method, the calculation is initiated based on the pinhole model assumption of the RGB webcam. The projection matrix is an integrated matrix that combines an intrinsic matrix of the camera and an extrinsic matrix which is comprised of a 3x3 rotation matrix and a 3x1 translation vector.

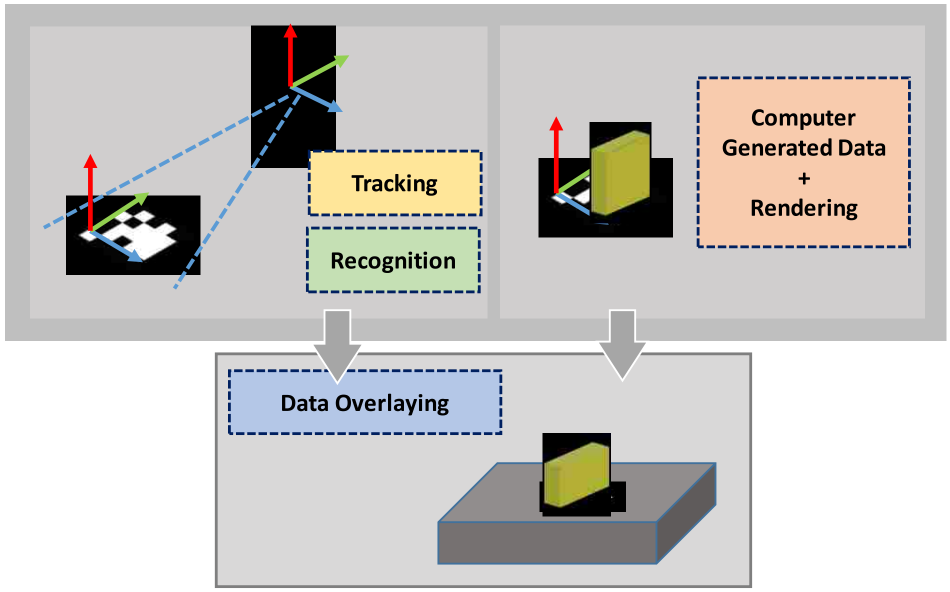

Figure 2.4. The pipeline of realizing AR. An attached marker and the features within the pattern are detected and recognized. The local coordinate system based on the markers is generated for estimating the relation between the marker and camera. The computer-generated data can be overlaid once the estimation is complete.

The equation of the camera pose estimation using homography is as follows:

$$\begin{bmatrix} u \\ v \\ 1 \end{bmatrix} = \begin{bmatrix} f_u & 0 & u_0 \\ 0 & f_v & v_0 \\ 0 & 0 & 1 \end{bmatrix} \begin{bmatrix} r_{11} & r_{12} & r_{13} & t_x \\ r_{21} & r_{22} & r_{23} & t_y \\ r_{31} & r_{32} & r_{33} & t_z \end{bmatrix} \begin{bmatrix} X_w \\ Y_w \\ Z_w \\ 1 \end{bmatrix} \tag{2}$$

where (u, v) are the coordinates in the 2D image plane of the display. The first term on the right side is the intrinsic matrix of the camera where (f_u, f_v) is the focal length and (u_0, v_0) is the center of the image plane. The second term represents the extrinsic matrix, where $r_{11} \dots r_{33}$ are the parameters of a rotation matrix and (t_x, t_y, t_z) is a translation vector. The third term is the world coordinate system based on the detected features of the target marker, which contains (X_w, Y_w, Z_w). The homography transformation the between two coordinate systems is illustrated in Figure 2.5.

Figure 2.5. The homography transformation between the two coordinate systems

Moreover, since Z_w in the world coordinate system can be set to zero as the Z_w of the feature points on the surface of the target marker is zero, providing a convience by replacing the third column of the extrinsic matrix to zero. Hence, the estimation equation is simplified as follows:

$$\begin{bmatrix} u \\ v \\ 1 \end{bmatrix} = \begin{bmatrix} h_{11} & h_{12} & h_{13} \\ h_{21} & h_{22} & h_{23} \\ h_{31} & h_{32} & h_{33} \end{bmatrix} \begin{bmatrix} X_w \\ Y_w \\ Z_w \end{bmatrix} \tag{3}$$

where the first term on the right side is the projection matrix and h_{11} ... h_{33} are its parameters. With the aid of the derived projection matrix, a 3D model can be accurately overlaid onto a 2D image plane as a composite view by using coordinate transformation. As an example, an AR composite view using homography is shown in Figure 2.6.

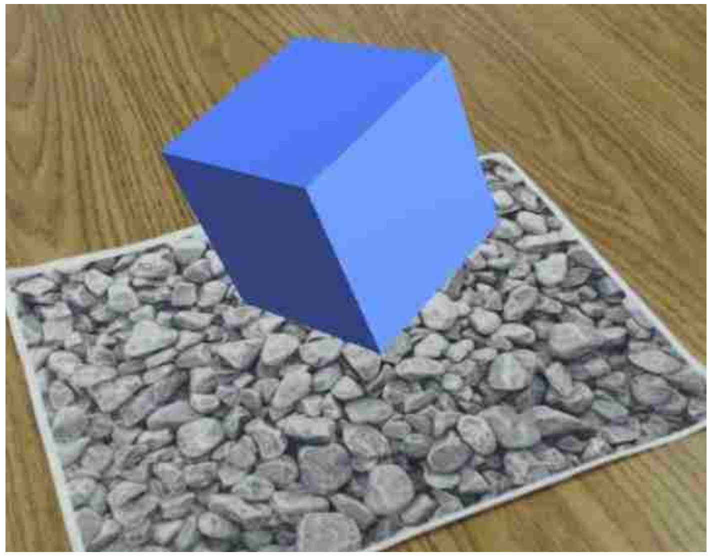

Figure 2.6. An example frame of an AR effect. A computer-generated cube is superimposed on the target marker using homography.

2.1.3. Multi-modal AR Realization. By utilizing homography, an augmented visual display can be realized to provide instructions for the assembly guidance through a composite view based on the coordinate system of the marker. Therefore, an AR visual queue can be established and deployed to a sequence of engineering assembly operations. With the aid of visual rendering, various types of detailed instructions are shown and augmented on the corresponding machine part through an AR display. Figure 2.7. shows an example frame of a multi-modal AR display for a mechanical assembly. To provide better understanding for training and performance, various types of visual AR renderings are provided in the system, e.g., texts, videos and 3D animations for instructions. Texts and videos are rendered through a 2D canvas of the display and AR 3D renderings are realized by superimposing 3D models with respect to the world coordinate system based on the target marker.

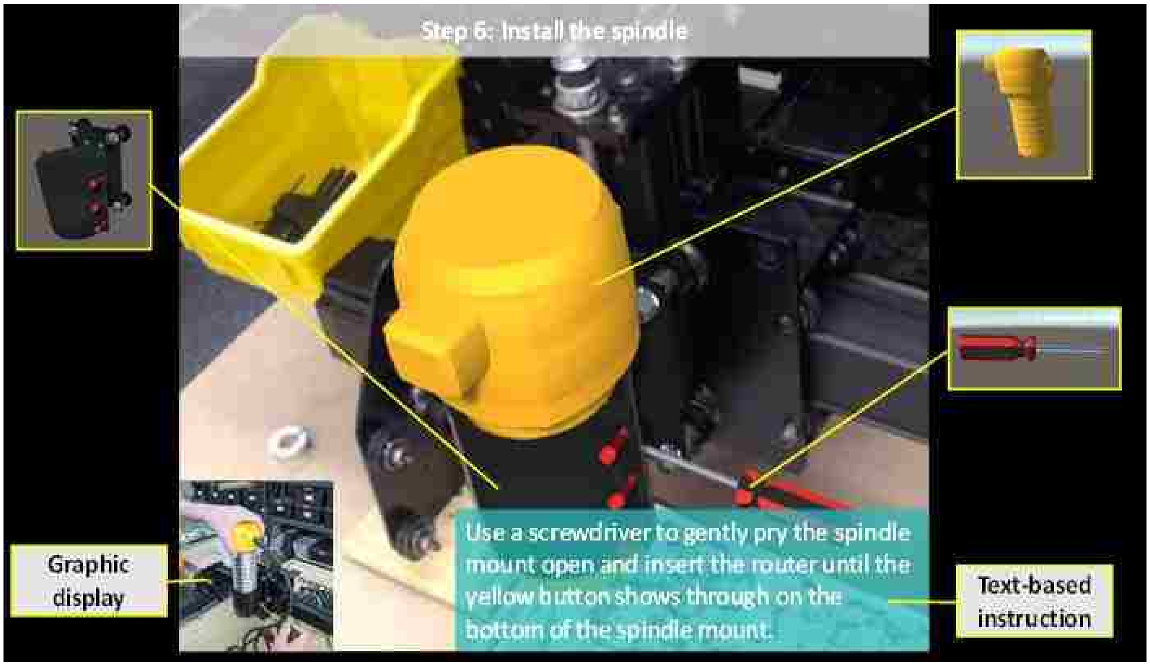

Figure 2.7. An example frame of multi-modal AR for a mechanical assembly. Multiple types of instructions are rendered through displays including text, graphics, and 3D animations.

Different colors and textures are arranged for different components, indicating their functional uses. In addition, animations and other spatially interactive behaviors of AR objects are realized via C# scripting in a Unity3D scene. With the augmented instructions informed in a visual display, subjects are able to sense and understand the operations through the provided information. However, without the tooling assistance message, the instructions are still limited when specific tools are required to finish the tasks correctly. To leverage it as a smart AR instructional system, a proposed tool detector with deep learning for decision making will be discussed in the following section.

2.2. DEEP LEARNING FOR TOOL DETECTION

During the manual assembly operation, how to efficiently secure every component in order to correctly assemble the entire product is crucial. To prevent from using wrong tools, a deep learning-based tool detector trained on a synthetic dataset is proposed, to help workers follow AR instructions. A webcam is mounted on top of the workbench to support workers in decision making. The camera captures video frames of the working area for the tool detector to classify and localize the target tools. The workflow of the proposed tool detector is presented in Figure 2.8.

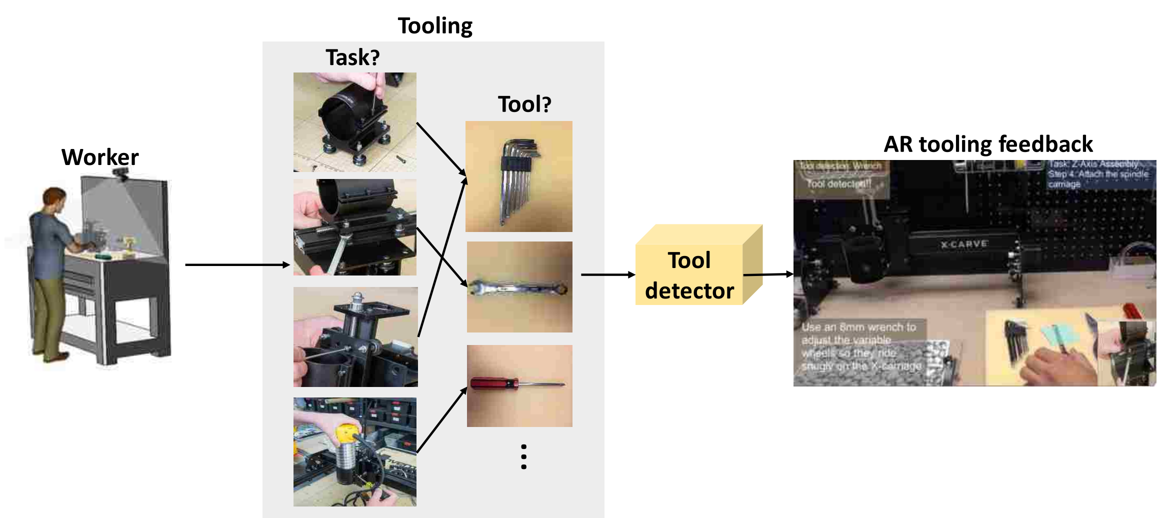

Figure 2.8. The system workflow of deep learning supported AR for tooling in assembly

2.2.1. Detection Approach. This section describes the tool detector development using a Region-based Convolutional Network (R-CNN) [28]. The detection approach incorporates a webcam that captures 2D frames of the working area and feeds the data into the model, which is trained on a synthetic dataset [30, 31] using Faster R-CNN [32] for target classification and localization. By using CNN [27], detailed features such as colors, contours and textures of the synthetic models are learned from the responded weights. Given an image or a video, the detection model is able to make inferences with the learned weights. Figure 2.9. illustrates the pipeline of R-CNN model trained on a synthetic dataset. By data augmentation, a detector for real tools is developed using CAD models for the tools, without the use of real tool image data.

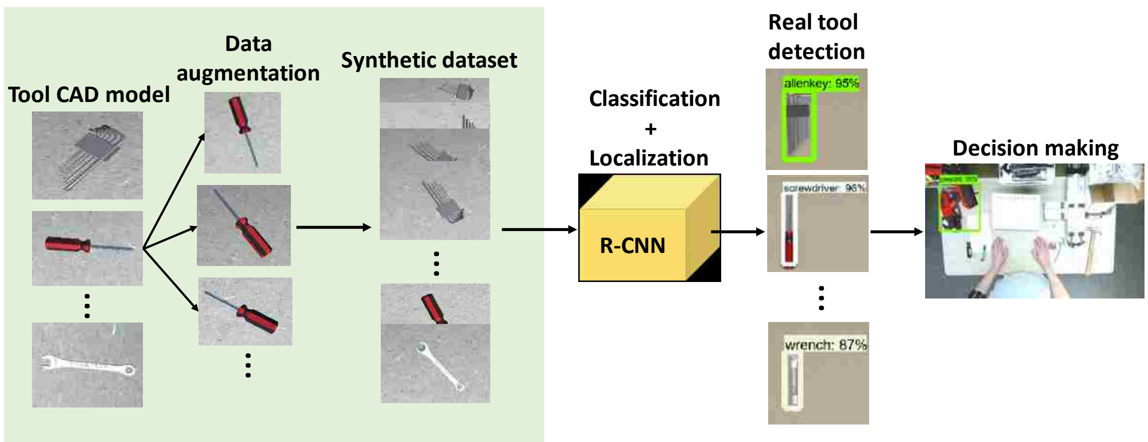

Figure 2.9. Synthetic dataset for R-CNN pipeline

2.2.2. Synthetic Tool Dataset. Considering the expensive cost of collecting real tool images and labeling the instances manually for a training model, a Computer-Aided Design (CAD) model based synthetic tool dataset is adopted. The objective is to classify and localize real tools in an assembly scenario by using only CAD models, which is efficient when training a new classifier and the amount of real data is limited [30]. The synthetic data for each class of tools is obtained by generating their CAD models with high similarity in colors, shapes and textures. Then the data is transformed to OBJ file format and imported to Unity3D engine. Five categories of CAD tools (Allen key, pliers, power drill, screwdriver, and wrench) are augmented to a scene by overlaying CAD models onto a 2D image background. After the model is augmented, the entire augmented scene is projected to another 2D image plane with a size of 1024×600 pixels for data generation. Figure 2.10. shows each class of tools in the dataset.

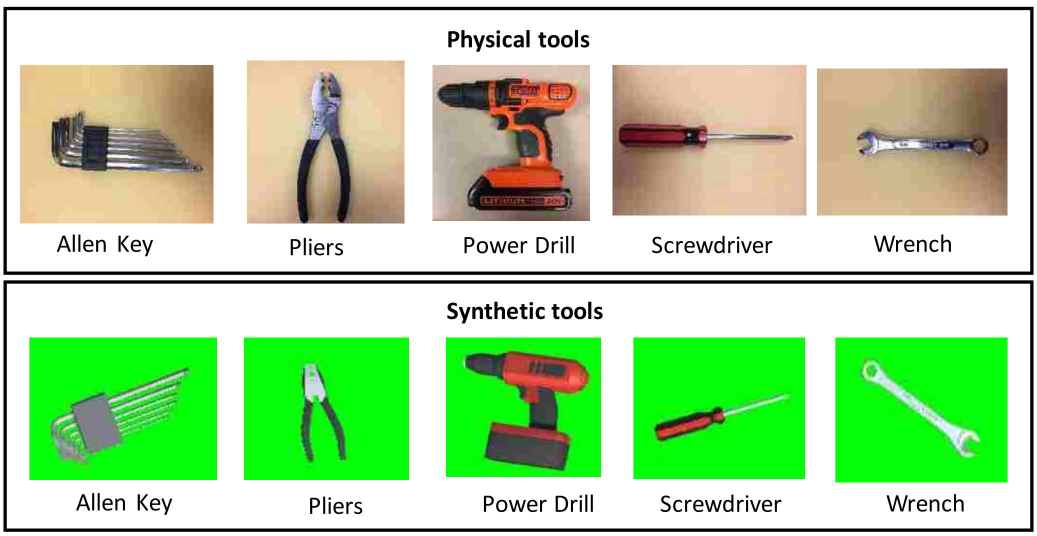

Figure 2.10. Synthetic data: 5 classes of CAD models for the synthetic tool dataset

To determine the scene for data augmentation and number of synthetic training images, the approach [31] tested on real PASCAL VOC2007 dataset [33] with the top mean Average Precision (mAP) using the configuration of RGB computer generated model with RGB image background is adopted. The number of images of each category for the peak result [31] is determined around 2000. In order to create an interclass variation for the classifier to reach higher performance on recognizing objects with different orientations within a scene [30, 31], a spatially varying generator is scripted and applied to models, which enables synthetic tools to constantly alter poses within the scene while the data is being collected. Figure 2.11. shows a synthetic tool that rotates about three different axes. By using the approach, an efficient data generation process is achieved. Once the augmentation is complete, a synthetic dataset with a resolution of 1024×600 of tools is developed for the deep learning model. Figure 2.12. illustrates the process of generating synthetic dataset for each class of tools using the data augmentation.

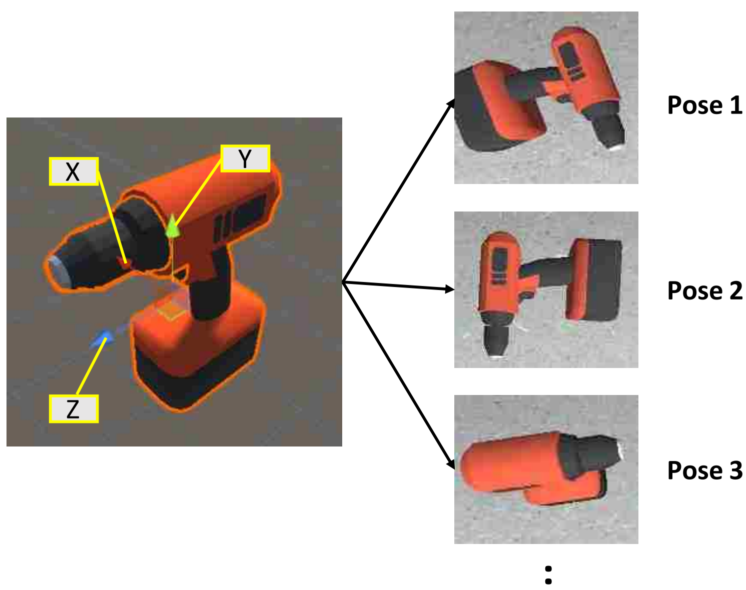

Figure 2.11. A synthetic tool rotates about three different axes. To create inter-class variation for purpose of higher recognition rate, a spatially varying generator is scripted for each class of synthetic tools.

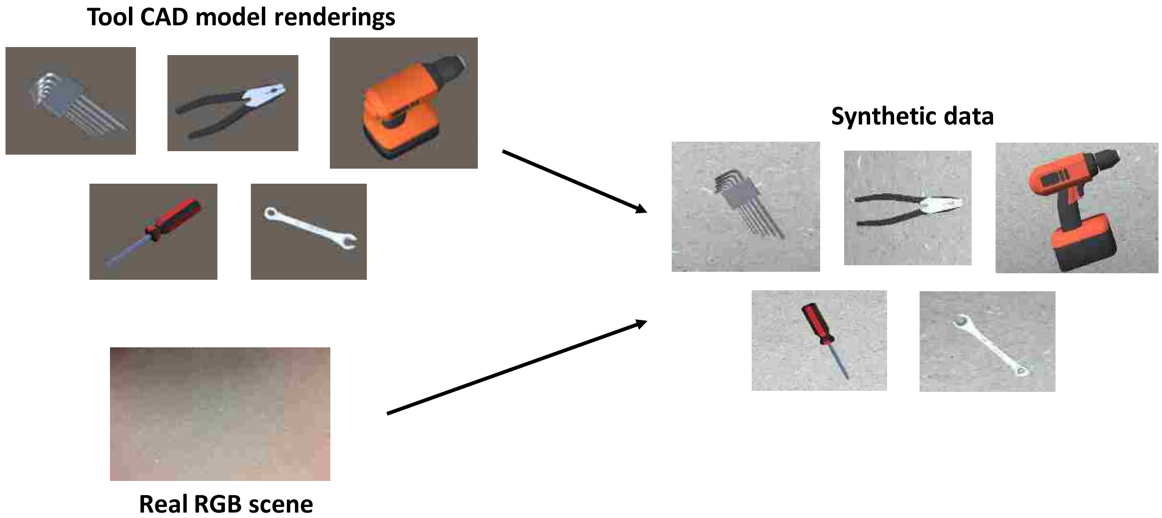

Figure 2.12. Synthetic data for R-CNN. By using data augmentation, the synthetic dataset can be generated with CAD models and an RGB scene (background).

2.2.3. Faster R-CNN. To build a tool detector, Faster R-CNN [32] is applied to achieve a higher recognition rate for high resolution images [34]. Given a video frame or an image, the detector is able to output classifications and localization results of tools. Faster R-CNN is developed based on a CNN and has been validated as a robust network for different levels of feature extraction [27]. After extracting features using a CNN, a Region Proposal Network (RPN) [32] is assigned for producing high quality proposals (bounding boxes) based on the extracted features of the convolutional feature map output from the CNN. RPN is a small network that generates proposals with multiple scales and aspect ratios and slide them through the convolutional feature map to detect objects. Figure 2.13. illustrates the generated region proposals with multiple scales and aspect ratios.

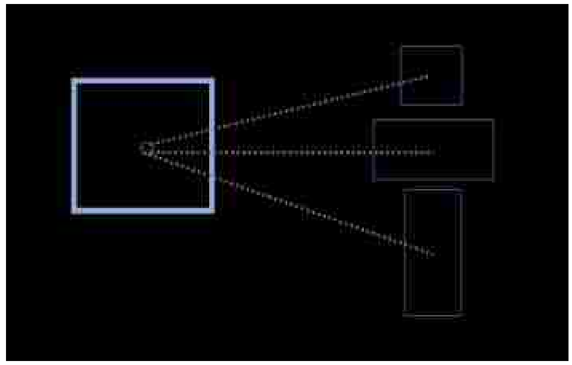

Figure 2.13. Region proposal network (RPN). An RPN generates multiple proposals and slides through the convolutional feature map output from a CNN.

Instead of feeding multiple unselected proposals computed from the external approach such as the selective search method [34] by merging adjacent pixels, RPN detects whether if there is an object in the proposal (bounding-box). It will pass forward for object classification and bounding-box regression only if there is an object detected within the proposal. Figure 2.14. summarizes the overall workflow of the Faster R-CNN architecture.

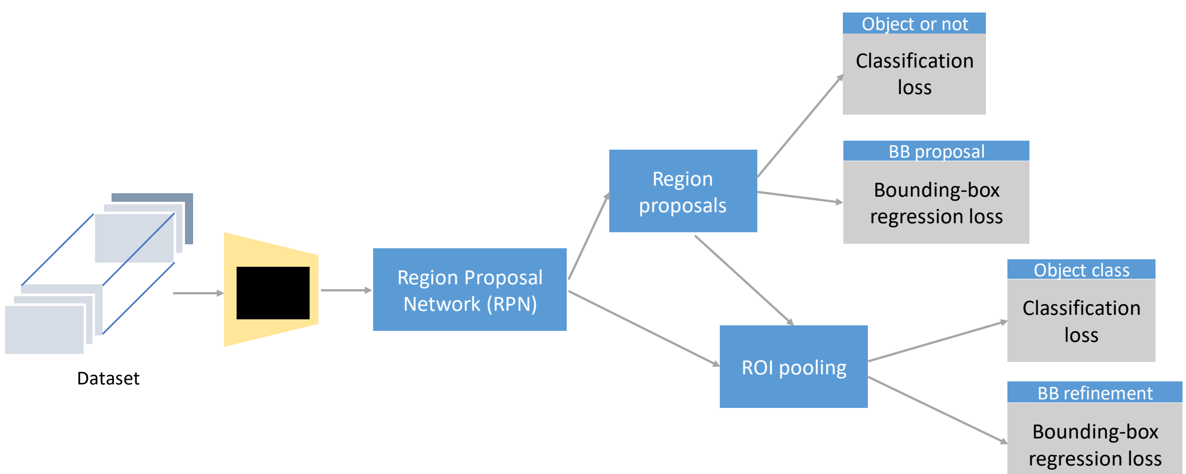

Figure 2.14. Faster R-CNN architecture.

An image frame is fed into a deep convolutional neural network for feature extraction. Then a Region Proposal Network is implemented to compute high-quality region proposals and pass forward to classification and bounding box regression. The model is trained by optimizing a set of weights, which minimizes the loss (cost) as the objective function while learning. The objective function is given below:

$$L(\{p_i\},\{t_i\}) = \frac{1}{N_{cls}}\sum_i L_{cls}(p_i,p_i^*) + \lambda\frac{1}{N_{reg}}\sum_i p_i^* L_{reg}(t_i,t_i^*) \tag{4}$$

The two terms on the right side represent classification and bounding-box regression, respectively. Symbol i indicates the index of proposals generated while using RPN. p_i^* is the binary classification label where it returns 1 when the object in the proposal is detected, and 0 otherwise. The bounding-box regression loss is activated only when $p_i^* = 1$, which contains t_i and t_i^*, attributing to four parameterized coordinates of the predicted box and the ground-truth box. After computing the object score using RPN, an ROI (Region of Interest) pooling layer is inserted to reduce the computation of the network by down-sampling the spatial size of the parameters. The classification of the detected object in the bounding-box is achieved by using a softmax function to predict classification scores over 5 classes of tools as follows:

$$P(y_i|x_i) = \frac{\exp(S_i)}{\sum_{k=1}^{5}\exp(S_k)} \tag{5}$$

where $P(y_i|x_i)$ is the predicted probability of a given image x_i and S_i, $i \in [1,5]$ is a 5-dimensional score vector representing the five different classes of tools. These five probability scores are normalized between zero and one as confidence scores that sum to one. For the bounding-box regression of the detected object, the bounding-box regressor is adopted from [28]. During training, N pairs of ground-truth boxes G and proposed boxes P are defined as training inputs, which are denoted as $\{(P^i, G^i)\}_{i=1,\dots,N}$, where P^i = $(P_x^i, P_y^i, P_w^i, P_h^i)$ represents the pixel coordinates of the center, width, and height of P^i. The ground-truth boxes are also represented as G^i = $(G_x^i, G_y^i, G_w^i, G_h^i)$. The training process is to learn the transformation and map the proposed box P to G, which is denoted as four functions: $d_x(P)$, $d_y(P)$, $d_w(P)$, $d_h(P)$. After the transformation is learned, the predicted box $\hat{G}$ can be generated by using the following transformations:

$$\hat{G}_x = P_w d_x(P) + P_x \tag{6}$$

$$\hat{G}_y = P_h d_y(P) + P_y \tag{7}$$

$$\hat{G}_w = P_w \exp(d_w(P)) \tag{8}$$

$$\hat{G}_x = P_h \exp(d_h(P)) \tag{9}$$

In the above equation, each $d_*(P)$ (where $*$ is one of x, y, h, w) is denoted as $w_*^T \phi(P)$, where $\phi(P)$ is modeled as a linear function of the features of a proposal and w_* is a vector of learnable model parameters [28]. After adopting the approach of object detection for AR tooling message, the system development and a designed experiment are determined for the evaluation, which will be discussed in the following sections.

2.3. SYSTEM OVERVIEW

For the smart AR instructional system development, two proposed systems are integrated through a connection of a User Datagram Protocol (UDP) socket. To provide ab AR tooling message, the detection results of the tool detector are transmitted through a scripted internet protocol (IP) listener to the AR domain, activating computer-generated visuals augmented on the corresponding tools for workers to locate. Figure 2.15. presents the workflow of the integrated system. Two RGB webcams are responsible for providing image data for multi-modal AR rendering and tool detection, respectively. The system integration is achieved with a UDP/IP socket, which is assigned for data transmission.

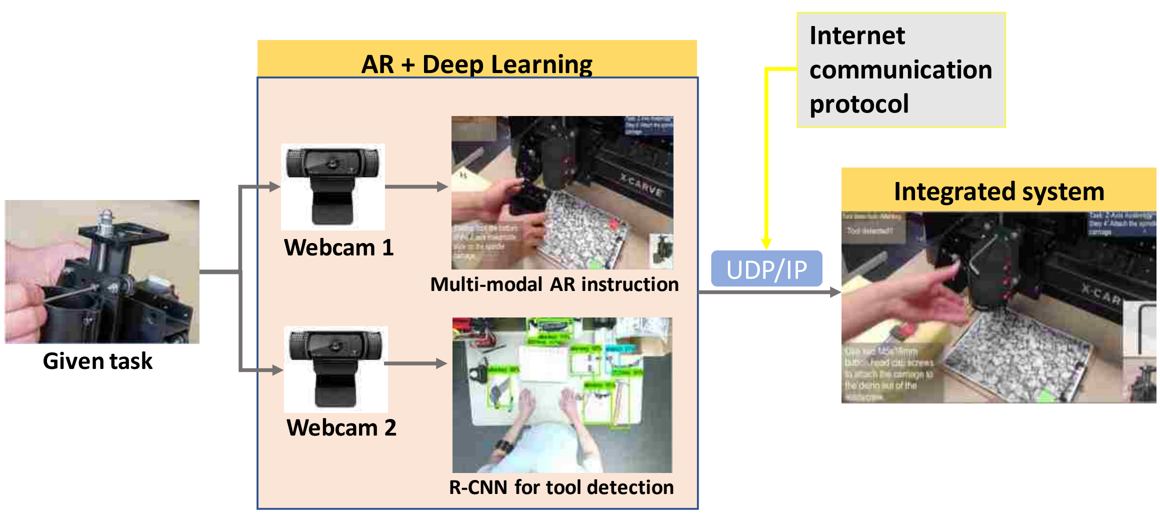

Figure 2.15. The workflow of the integrated system

Since the integrated system runs with two different webcams, mapping the coordinates from the 2D image plane of R-CNN to the 2D image frame of AR is required. An affine transformation is utilized for coordinate transformation. The function of the transformation is:

$$\begin{bmatrix} x' \\ y' \\ w' \end{bmatrix} = \begin{bmatrix} a1 & a2 & a3 \\ a4 & a5 & a6 \\ 0 & 0 & 1 \end{bmatrix} \begin{bmatrix} x \\ y \\ w \end{bmatrix} \tag{10}$$

where (x, y, w) represents three center points of three drawn bounding-boxes in the image plane of R-CNN, respectively. (x', y', w') indicates three corresponding points in a video frame of AR. $a1 \ldots a6$ are the target parameters of the transformation matrix. Once the transformation matrix is computed through two sets of points from two different coordinate systems, the coordinate transformation can be achieved through the derived matrix. Figure 2.16. shows the workflow of mapping an AR visual with coordinate transformation.

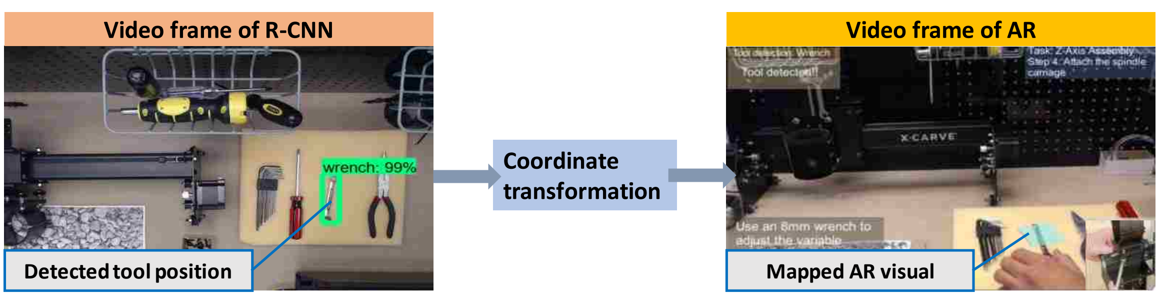

Figure 2.16. The derived transformation matrix maps the coordinate to a video frame of AR. By using affine transformation, the coordinates of the detected tool in R-CNN can be converted to the coordinates in AR through a computed transformation matrix.

3. EXPERIMENT

3.1. EXPERIMENTAL SETUP

To evaluate the performance of the proposed system, an experimental setup with two webcams and one monitor for the on-site display is designed. One top-down webcam is mounted on top of the workbench as a surveillance camera to capture the working area for tool detection and the other webcam is situated on a neighboring tripod for the AR display. To simulate the assembly scenario in the industry, a given toolkit for the assembly task is arranged aside. A photo of the full workstation setup for the designed experiment is shown in Figure 3.1.

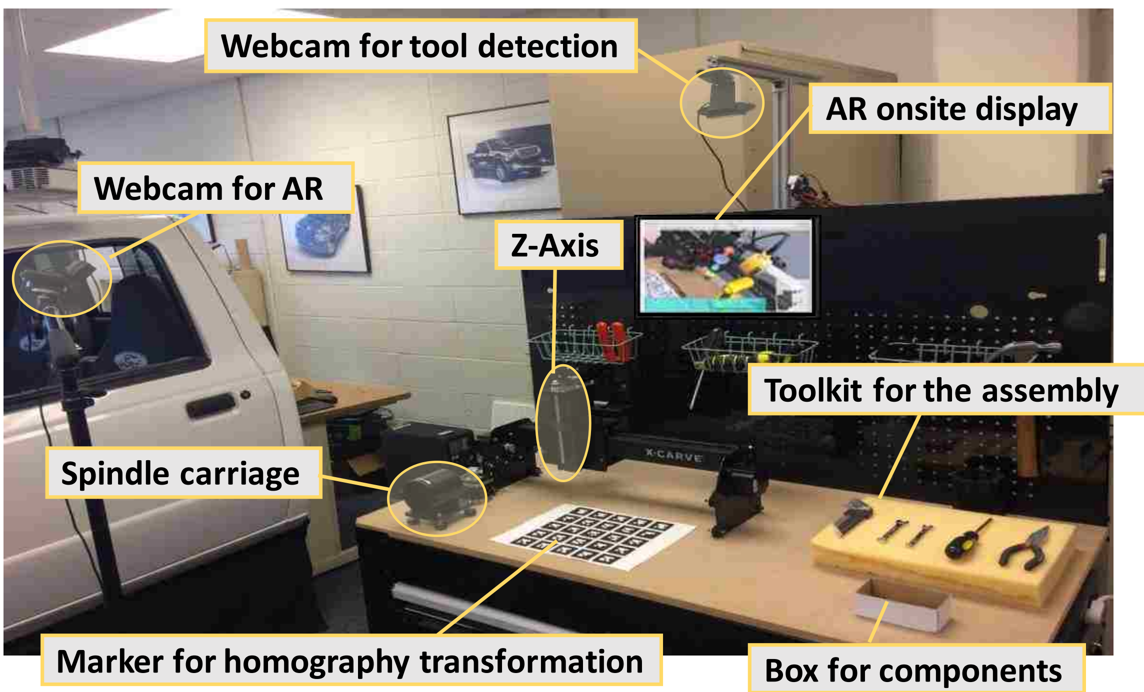

Figure 3.1. A workstation setup for the experiment. One webcam is mounted on top of the workbench as a surveillance camera and the other camera is situated on a neighboring tripod. A monitor for the onsite display is attached to the workbench. All the required components and the toolkit are also arranged aside.

For the experiment, a spindle installation of a consumer grade CNC carving machine (Inventables: X-Carve 750mm) is decided, which requires instructional guidance and mechanical knowledge to finish the assembly correctly. The goal of the assembly task is to install the spindle onto the z-axis mechanism with provided components and tools. The photos of the z-axis mechanism and the installed spindle are shown in Figure 3.2. and 3.3., respectively.

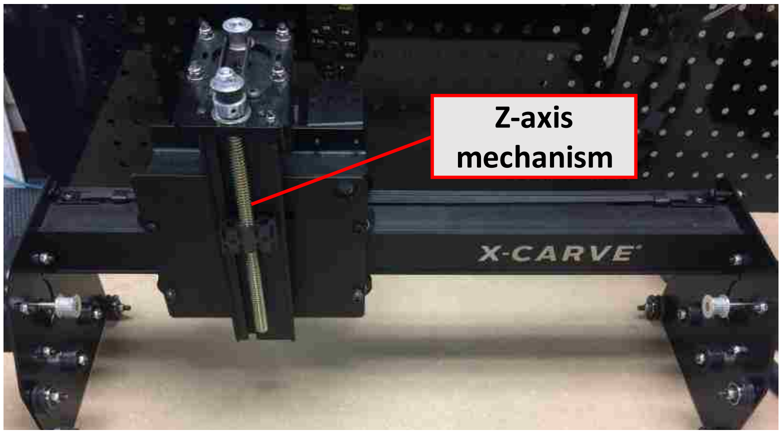

Figure 3.2. The z-axis mechanism of the spindle assembly

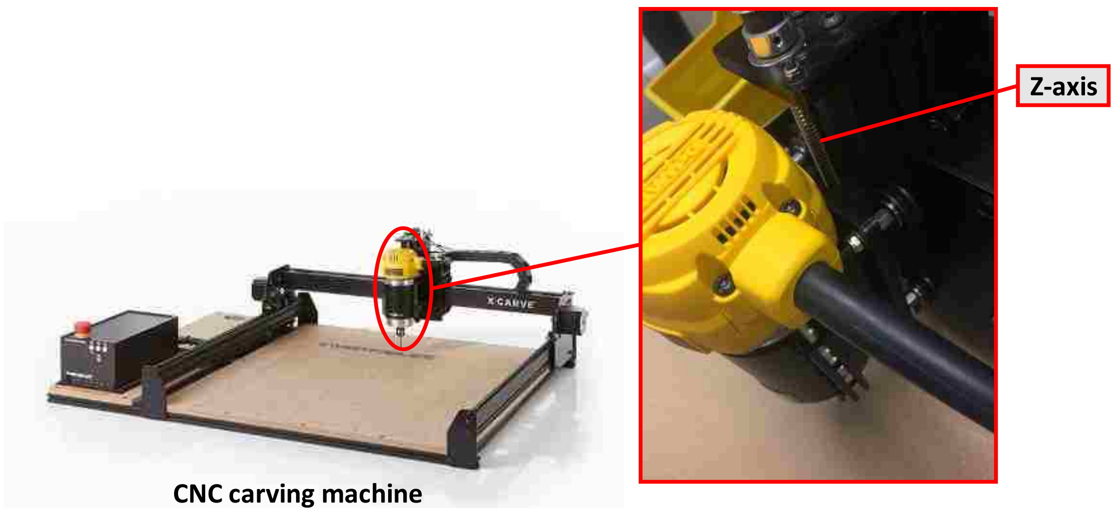

Figure 3.3. The installed spindle with the z-axis

The spindle installation contains seven steps. Each step consists of multiple operations that require different tools or components for the assembly. The summarized information provided on the instructional manual is given in Table 3.1. along with its graphical illustrations [36]. With the defined engineering tasks, the experimental setup is determined. The experimental procedure will be discussed in the next section.

Table 3.1. The spindle assembly task [36]

Step No.	Name	Graphic instruction	Tool/Component	Instruction
1	Insert spindle carriage clamping bolts		Tool: Allen key Component: Socket head screw M4 x 16mm	Thread in three of the M4 x 16mm socket head screws.
2	Attach spindle Carriage to Z-axis (1)		None	Starting from the bottom of the Z axis, slide on the spindle carriage.
3	Attach spindle Carriage to Z-axis (2)		Tool: Allen key Component: Button head cap screw M5 x 16mm	Use two M5x16mm button head cap screws to attach the carriage to the delrin nut of the leadscrew.
4	Attach spindle Carriage to Z-axis (3)		Tool: 8mm wrench Component: Lock nut	Use an 8mm wrench to adjust the variable wheels so they ride snugly on the carriage, but not so tight that they cannot be moved by hand.

Table 3.1. The spindle assembly task [36] (Cont.)

5	Attach Z-axis home switch		Tool: Allen key & pliers Component: screw, nut	Thread on an M3 nylock nut and tighten it against the plate with either a 5.5mm socket as pictured here, or with the appropriate wrench/pliers.
6	Spindle (1)		Tool: Screw driver Component: Spindle	Use a screwdriver or other prying tool to gently pry the spindle mount open and insert the router until the yellow button shows through on the bottom of the spindle mount.
7	Spindle (2)		Tool: Allen key Component: Socket head screw M4 x 16mm	Tighten the three M4x16mm screws to hold the router in place.

3.2. SYSTEM EVALUATION

The completion time and number of errors are the most crucial indicators to evaluate the performance of an assembly operation [37], thus two kinds of data are recorded for evaluation.

3.2.1. Subject Selection and Testing. To collect data, 20 physically and cognitively healthy subjects, including male and female graduate students and faculties at the average age of 28 at Missouri S&T are recruited. All the subjects are confirmed having no prior knowledge of the experiment. They are divided into two groups of 10 subjects to conduct the experiment. One group is asked to perform the assembly by using the paper manual available from the manufacturer, and the other group performs the assembly with the smart AR system developed. During the experiment, each of the subjects is asked to stand in front of the workbench to perform the assembly task. The elapsed time is recorded with a stopwatch and the number and type of errors is documented if a mistake occurs. Three types of assembly errors are in Table 3.2, which are considered the most generic errors in a mechanical manual assembly process [37].

Table 3.2. Three types of assembly errors

No.	Error type	Description
1	Tool/Part selection	Misuse the tool/part to conduct the assembly
2	Assembly order	Assemble with incorrect sequence
3	Installation	Assemble with incorrect installation/fixation

As shown in Table 3.2., the tool/part selection error occurs when a subject misuses incorrect tool/part to perform the assembly tasks. The assembly order error could be caused by mistakenly following the sequence of instructional guidance or assemble components in an incorrect order. The installation error takes place when a subject install parts with incorrect fixation, which includes mismatching components or securing them improperly.

3.2.2. Evaluation Metric. For the quantitative evaluation of the tool detector developed, the Intersection over Union (IoU) metric [33] is adopted. If a ground-truth box and a predicted box are overlapped by 0.5 or larger, then the prediction is a True Positive (TP). The formula is denoted by:

$$a_o = \frac{area(B_p \cap B_{gt})}{area(B_p \cup B_{gt})} \tag{11}$$

where a_o represents the overlap ratio between the ground-truth box B_{gt} and predicted box B_p. $B_p \cap B_{gt}$ and $B_p \cup B_{gt}$ are the intersection and union of them, respectively. Figure 3.4. provides an illustration of IoU.

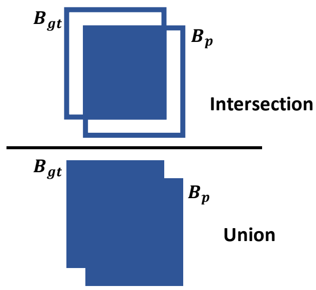

Figure 3.4. The Intersection over Union (IoU)

To calculate Average Precision (AP), the Precision metric [33] is defined as:

$$Precision = \frac{TP}{TP + FP} \tag{12}$$

where True Positive (TP) represents an instance from the target class that is correctly classified as the target class. False Positive (FP) represents an instance from a class other than the target class that is misclassified as the target class.

4. RESULTS

In this section, the experimental results are discussed, including the tool detector and smart AR rendering, as well as the evaluation of the integrated system. Figures 4.1. and 4.2. show two snapshots of two subjects performing the assembly experiment using two different methods (paper manual vs. Smart AR) for system evaluation.

Figure 4.1. A subject is performing the experiment using the paper manual

Figure 4.2. A subject is performing the experiment using the Smart AR system

4.1. TOOL DETECTOR AND SMART AR RENDERING

The tool detector is achieved by fine-tuning a Faster R-CNN pre-trained model using TensorFlow object detection API with approximately 64K iterations and the learning rate of 3×10^{-4}. The classification layer of the Faster R-CNN algorithm is modified to output softmax probability scores in [0, 1] over 5 classes of tools. Once the tools are detected in a video frame, the detector draws bounding-boxes around the located tools using bounding box regression. Figure 4.3. shows two example detection results of all the classes of tools of the experimental setup.

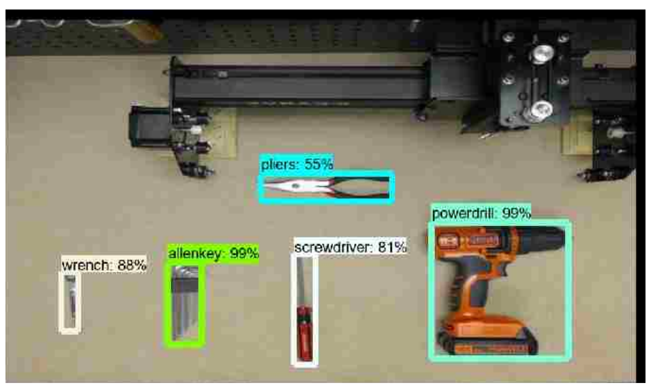

(a)

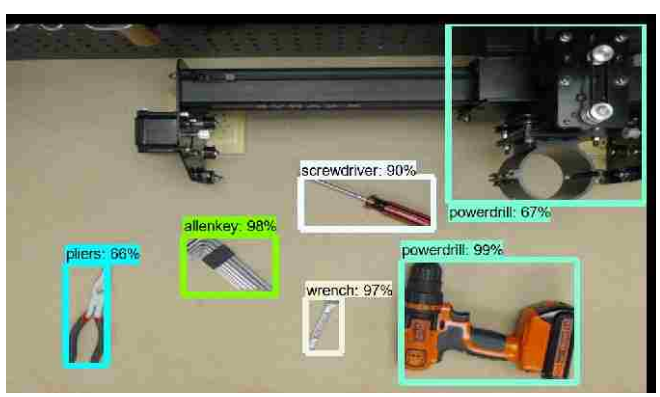

(b)

Figure 4.3. Tool detection using Faster R-CNN with a surveillance camera

The tool detection results show that, the tool detector is able to classify and localize the physical of real tool target with various poses, which demonstrates the viability of CNN using CAD data augmentation. Figure 4.4. shows the results of detecting real tools with different orientations.

Figure 4.4. The results of detecting real tools with various orientations

Table 4.1 shows the precision of detecting real tools using the developed tool detector for Intersection over Union (IoU) evaluation on a real tool dataset captured from the surveillance camera with a resolution of 1024×600.

Table 4.1. Average Precision on detecting different real tools

Tool	Average Precision
Allen Key	64.7%
Pliers	95.9%
Power drill	72.4%
Screwdriver	97.2%
Wrench	93.5%
mean	84.7%

The mean of the Average Precision for the five tools is 84.7%, indicating a strong performance of utilizing synthetic data for real object detection. As shown in Table 4.1., screwdriver outperforms all the other tools, likely due to the unique tool shape and color of the grip. Allen key has the lowest score of precision, which is possibly caused by its shape and color that may result in a confusion with other non-tool objects in the background. Figure 4.5. shows the example frames of False Positive (FP), which lead to decrease in precision of predicting Allen key and power drill. Two irrelevant objects in the bounding-boxes are misclassified as Allen key and power drill with the detection scores of 51% and 53% that are output from the softmax function, indicating a lower confidence of predicted classes inside the bounding-boxes. Clearly, the background affects the precision of tool recognition as False Positive occurs. Also, a decrease in the precision there are more objects within the captured frame.

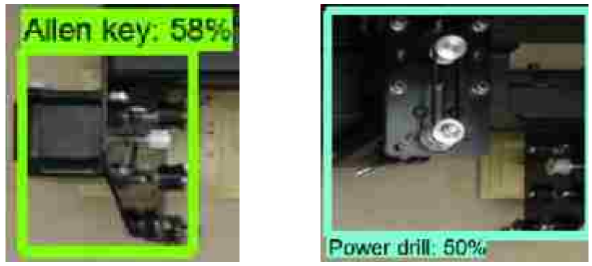

Figure 4.5. Example frames of False Positive (FP). The misclassification occurs when video frames include non-tool objects in the background

According to the assembly requirements, subjects need to fasten the components with the required tools while following the AR assembly instruction. By combing multi-modal AR rendering and the tool detector, AR visuals of tooling message are provided. In Figure 4.6. and 4.7., two example frames representing two instances of the integrated system during the assembly are shown. The red rectangle in the figure highlights the position of the tool generated by the of tool detector while the AR assembly instructions are also rendered in each frame, displaying a current state of the operation.

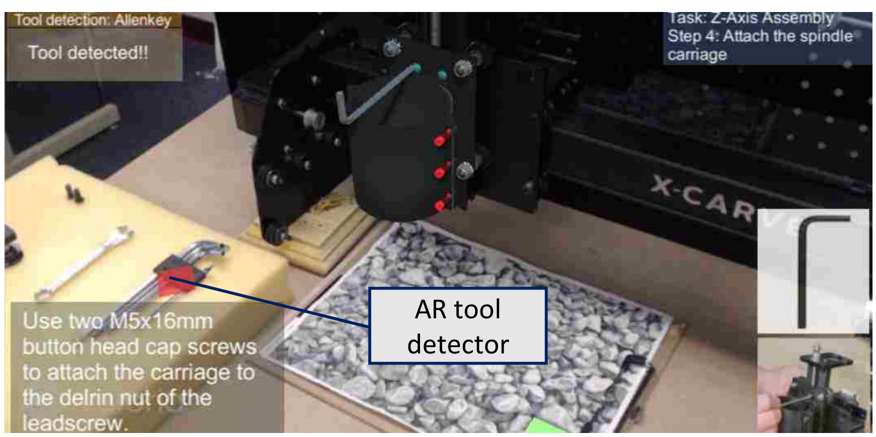

Figure 4.6. AR integrated with the tool detector for Step 3 of the assembly task

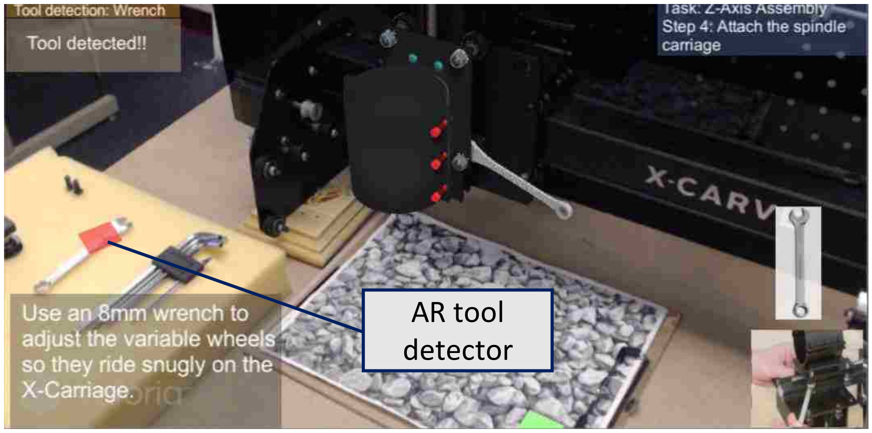

Figure 4.7. AR integrated with the tool detector for Step 4 of the assembly task

4.2. SYSTEM EVALUATION RESULT AND DISCUSSION

To evaluate the validity of the integrated system, assembly completion time and number of errors of the two groups are presented in Tables 4.2. and 4.3.

Table 4.2. Results of the group using paper manual

Subject	Gender	Total number of errors	Number of error type 1	Number of error type 2	Number of error type 3	Completion time (s)
1	Male	6	1	1	4	725
2	Male	2			2	616
3	Female	3		1	2	729
4	Male	2			2	596
5	Male	4	2		2	1057
6	Male	6	1		5	712
7	Male	2	1		1	689
8	Male	3	3			605
9	Male	3	1		2	708
10	Female	3	2		1	1113
Mean	—	34	—	—	—	755

Table 4.3. Results of the group using smart AR instructional system

Subject	Gender	Total number of errors	Number of error type 1	Number of error type 2	Number of error type 3	Completion time (s)
11	Male	1			1	424
12	Male	2			2	359
13	Male	2			2	531
14	Male	1			1	531
15	Male	5	1		4	600
16	Female	4			4	914
17	Male	2	1		1	421
18	Male	1			1	573
19	Male	3			3	413
20	Female	2	1		1	278
Mean	—	23	—	—	—	504.4

As shown above, the two results of using different instructional guidance are recorded and analyzed. Also, Figures 4.8. and 4.9. compare the mean completion time and the mean number of errors using ANOVA for the two groups. By following the smart AR instruction, the completion time is reduced by 33.2%, and the assembly error of using the proposed system is reduced by 32.4% comparing to the conventional method of using a paper manual. These reductions are mainly due to the paper manual difficult to interpret, resulting in the subject spending more time on retrials and understanding the instructions in order to assemble correctly.

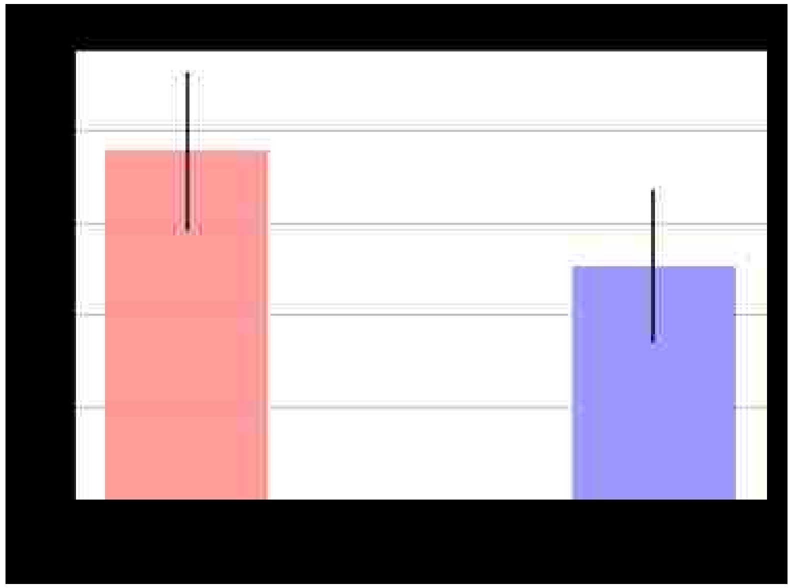

Figure 4.8. The mean completion time of two groups

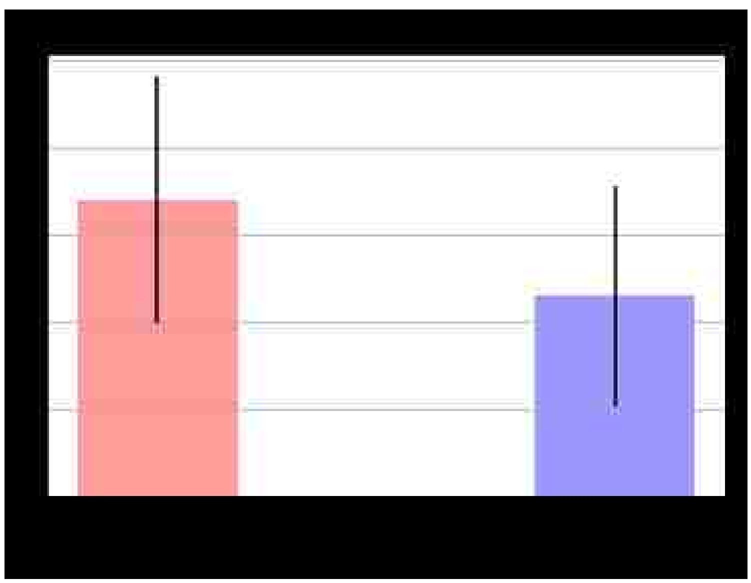

Figure 4.9. The mean number of errors of two groups

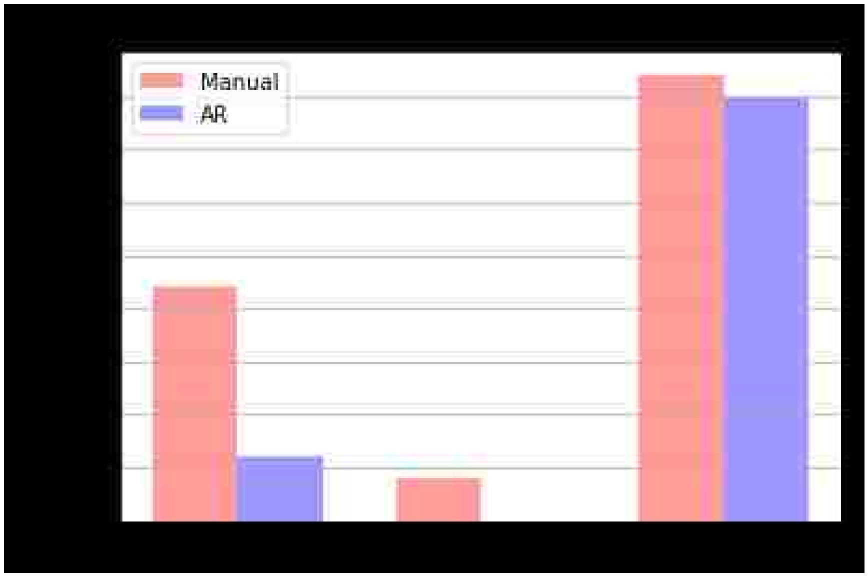

Figure 4.10. The comparison of three types of error

Table 4.4. Percentage reduction for each type of errors using the AR instruction

Error type	1	2	3
Reduction	72.7%	100%	4.8%

Figure 4.10. and Table 4.4. present a comparison and the percentage of reduction for each type of errors with the assistance of the smart AR instructional system. As shown, two types of errors including tool/part selection (Type 1) and assembly sequential order (Type 2) errors are reduced by 72.7% and 100% respectively, with the aid of dynamic AR queue and tool detection. The installation error is recorded as the most error-prone from both groups, which also has the least improvement in error reduction with the use of AR assistance. Tables 4.5. and 4.6. present a more detailed summary of errors from the two different groups, which contain error type and how the errors are made in each step along with the documented description of the spindle assembly task.

Table 4.5. Error analysis of the experiment with the paper manual

Type / Step	1	2	3	Description
1	3	1	8	Type 1: Should use an Allen key, instead of a screwdriver Type 2: Incorrect assembly sequence Type 3: Should leave the screws loose
2			12	Type 3: Mismatch the carriage and the track
3	2	1		Type 1: Should use an Allen key, instead of a screwdriver Type 2: Should tighten the screws first
4			1	Type 3: Securing incorrect nuts
5			1	Type 3: Apply too much torque while securing the screw
6	1			Type 1: Should use a screwdriver, instead of a screwdriver
7	4			Type 1: Should use an Allen key, instead of a screwdriver

Table 4.6. Error analysis of the experiment with the smart AR system

Type / Step	1	2	3	Description
1			3	Type 3: Should leave the screws loose
2			12	Type 3: Mismatch the carriage and the track
3	2		2	Type 1: Should use an Allen key, instead of a screwdriver Type 3: Mismatch the carriage and the delrin nut
5	1			Type 1: Should use pliers, instead of a wrench
6			3	Type 3: Pry at an incorrect position

According to the analysis, Type 3 errors in Step 2 are the most recorded type of error using either the manual or the smart AR system. Examining those errors provides the following insight: although AR rendering is able to provide spatial information regarding the geometry of the parts to be assembled, improvement in the AR system still needed in order to help workers comprehend the relationships among different parts, e.g., matching a V-wheel mechanism of the carriage to the track on the z-axis. Figure 4.11. shows two snapshots of two subjects performing Step 2 with two different guiding instructions in the assembly process. Moreover, a quality assembly should be finished in one-time installation to avoid damage from retrials. Figure 4.12. shows a snapshot of the wear on a V-wheel mechanism that is damaged by repeated failure at mounting the carriage on the z-axis track from Step 2, which may downgrade the quality of the assembly. The proposed AR guiding system can be further improved based on the recorded errors.

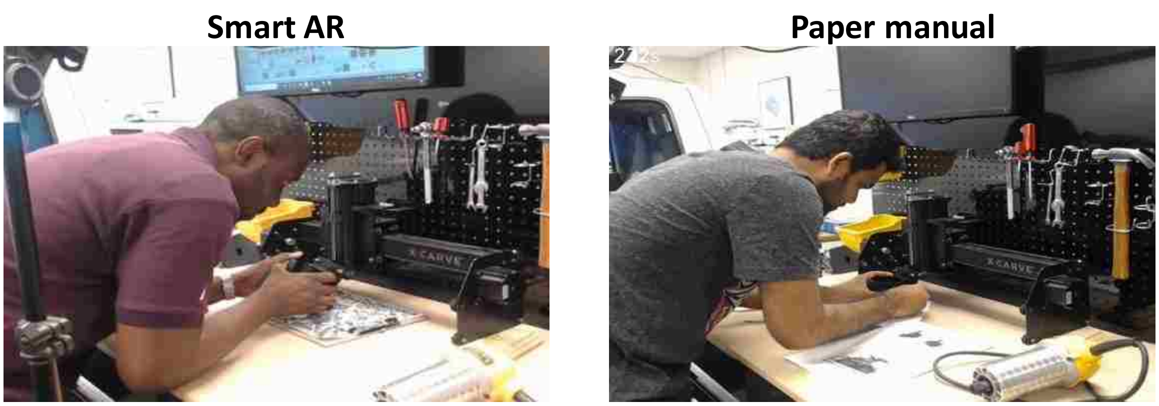

Figure 4.11. Two subjects perform Step 2 with two different instructional guidance

Figure 4.12. The wear of a V-wheel mechanism caused by the installation error

To sum up, the experimental results indicate a considerable improvement in the assembly performance by implementing smart AR instructions to mechanical assembly tasks in comparison to the conventional method of using paper manuals. The developed AR guiding system has demonstrated the promising potential of integrating AR and deep learning for manual assembly.

5. CONCLUSION

This thesis presents the development of a smart Augmented Reality (AR) worker assembly instructional system aiming at improving the worker's performance by incorporating deep learning into augmented reality for mechanical assembly. The developed system consists of multi-modal AR instructions allowing workers to respond intuitively and a tool detector using deep learning. The multi-modal AR rendering that provides various types of on-site instructions (texts, videos, 3D animations) is realized with the aid of homography in Unity3D. The tool detector is developed with a Faster R-CNN trained on a CAD based synthetic tool dataset, which is able to classify and localize real physical tools with a mean Average Precision of 84.7%. Evaluating the integrated smart AR system on the assembly of a motor spindle shows the result that it reduces the assembly completion time by 33.2% and assembly errors by 32.4%. Thus, the integrated AR system has demonstrated its potential in assisting human operators when performing complex assembly tasks.

APPENDIX

AUGMENTED REALITY IN UNITY3D AND UDP SOCKET OPERATION

1. UNITY3D

Unity3D is a gaming engine developed by Unity Technologies that allows users to design and build games that comprise multiple scenes with desired models and various visual effects including 2D and 3D graphics, textures, lighting and shading. To apply the CAD model to the scene, users need to convert the file format so it could be imported to Unity3D and then simply load to the scene by using import asset from the drop-down menu. The imported 3D model would be categorized as game objects and be sorted on the hierarchy panel once it has been assigned to the scene. Figure A.1 shows the designed part modeled in the CAD software NX 12 [38] and Figure A.2 shows the drop-down menu for importing process.

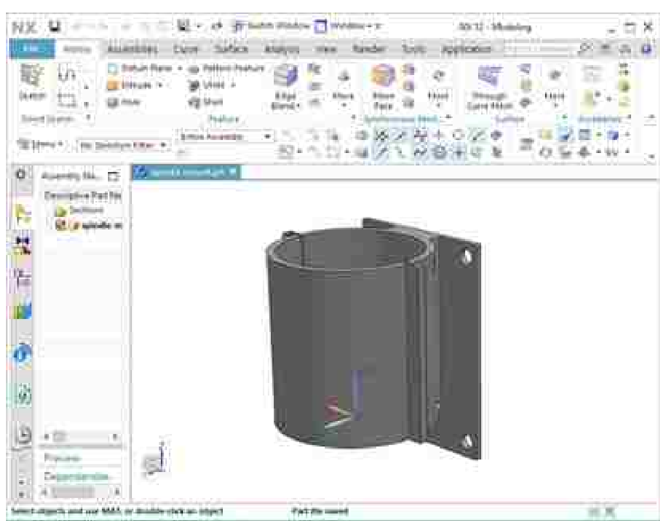

Figure A.1. The deigned CAD model of the spindle carriage

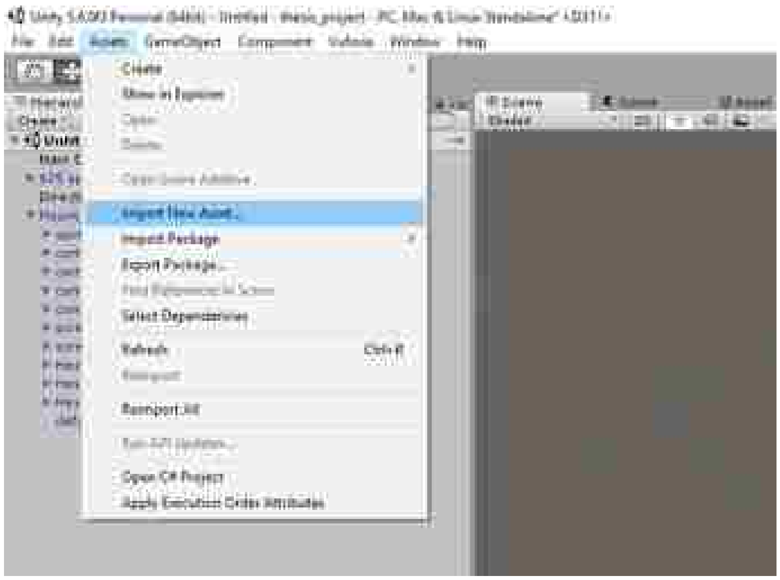

Figure A.2. The deigned CAD model of the spindle carriage

Every game object in the scene can be arranged by assigning specific positions, angles and scales as it is embedded with a Transform property. Figure A.3 shows the imported deigned model in the Unity3D scene and its spatial information regarding to the coordinate system of the scene.

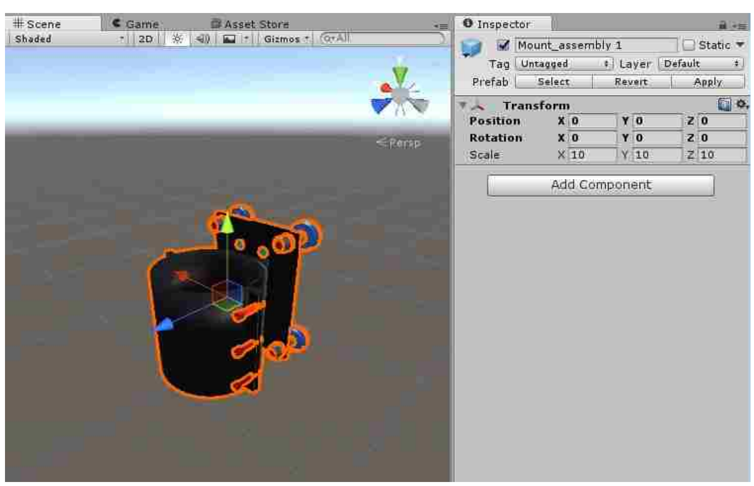

Figure A.3. The imported 3D CAD model of spindle carriage

In addition, the engine platform also supports scripting via programming languages such as C# and JavaScript, enabling the physics and dynamic behavior of the game object. The overall game scene and its description is illustrated in Figure A.4. After the desired scene is developed, the user can launch the play mode to activate all of the settings for the game objects. Also, the console of the main project panel could show the update for the current status while under the play mode.

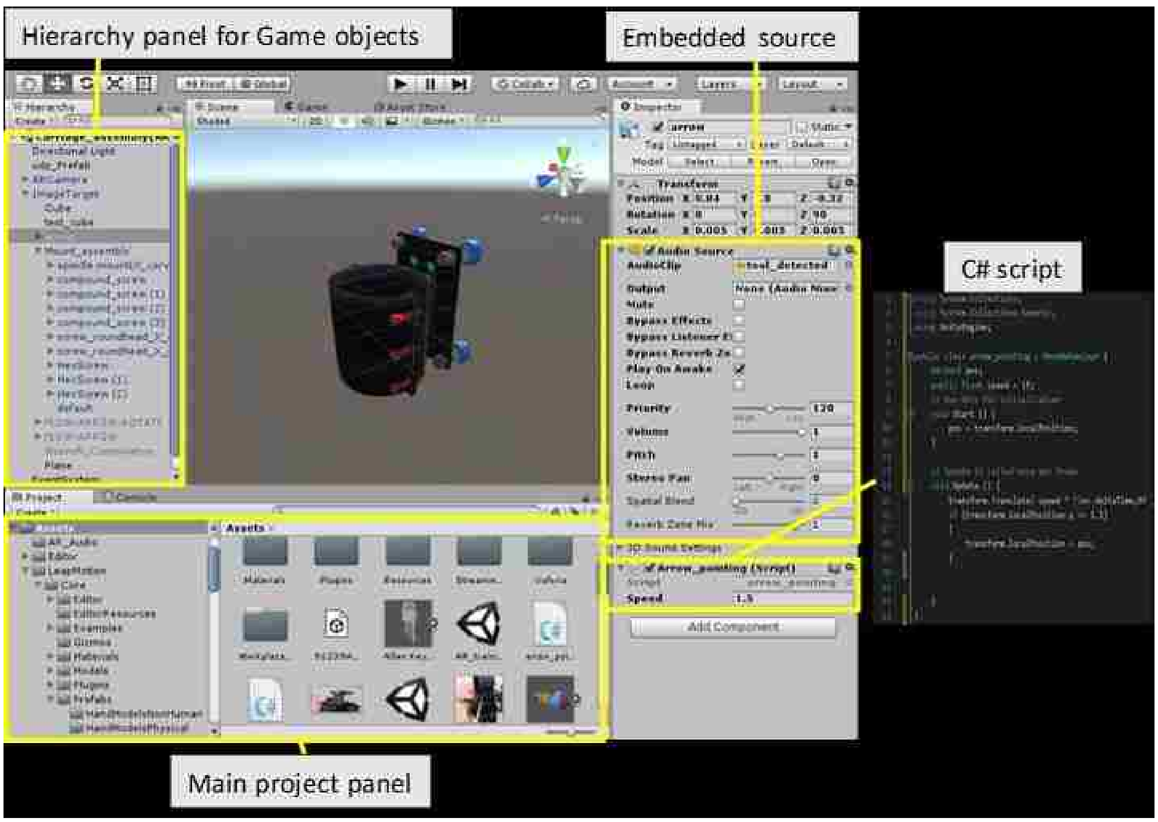

Figure A.5. The imported CAD model of spindle carriage.

2. VUFORIA

Vuforia is a Software Development Kit (SDK) for Augmented Reality that can be directly applied as an asset for Unity3D. It provides the functionalities that offer target recognition and tracking through the built-in Computer Vision (CV) algorithm, enabling users to situate Computer Generated (CG) 3D visuals with respect to the world coordinates as data registration. To define targets, users can assign markers by importing

the desired images for data augmentation with a variety of configurations for marker-based AR. Moreover, the SDK has included several prefabs which provide a wide variety of uses as needed, e.g., virtual button prefab for human-computer interface without physical hardwire needed. Figure A.5. shows the applicable prefabs of Vuforia in Unity3D.

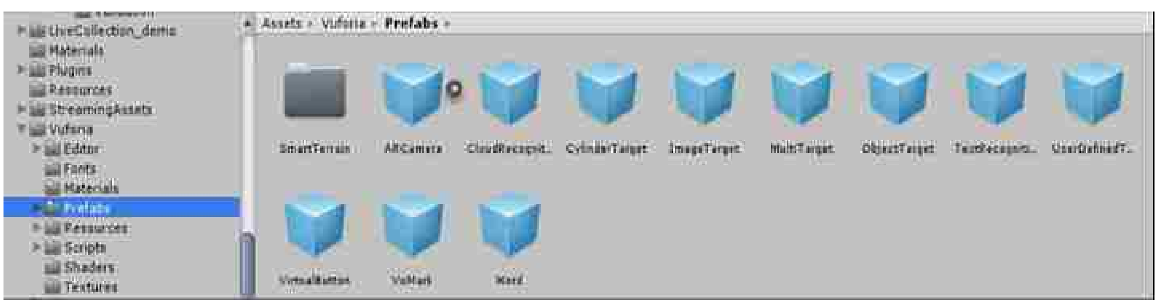

Figure A.6. Vuforia prefab in Unity3D

To realize the AR effect, two prefabs are required for data augmentation, which are ARCamera and ImageTarget prefabs. The ARCamera prefab would need to be activated using provided license key from the developer portal, so the marker data can be loaded in through the embedded Vuforia Behavior script. Once the data has been loaded, the user will need to activate the Image Target Behavior of the ImageTarget prefab by setting the dataset and image target. After the setting is finished, the augmented view can be visualized through the display while the marker is being captured by the camera. Figures A.6. and A.7. illustrate the two prefabs and the AR visual.

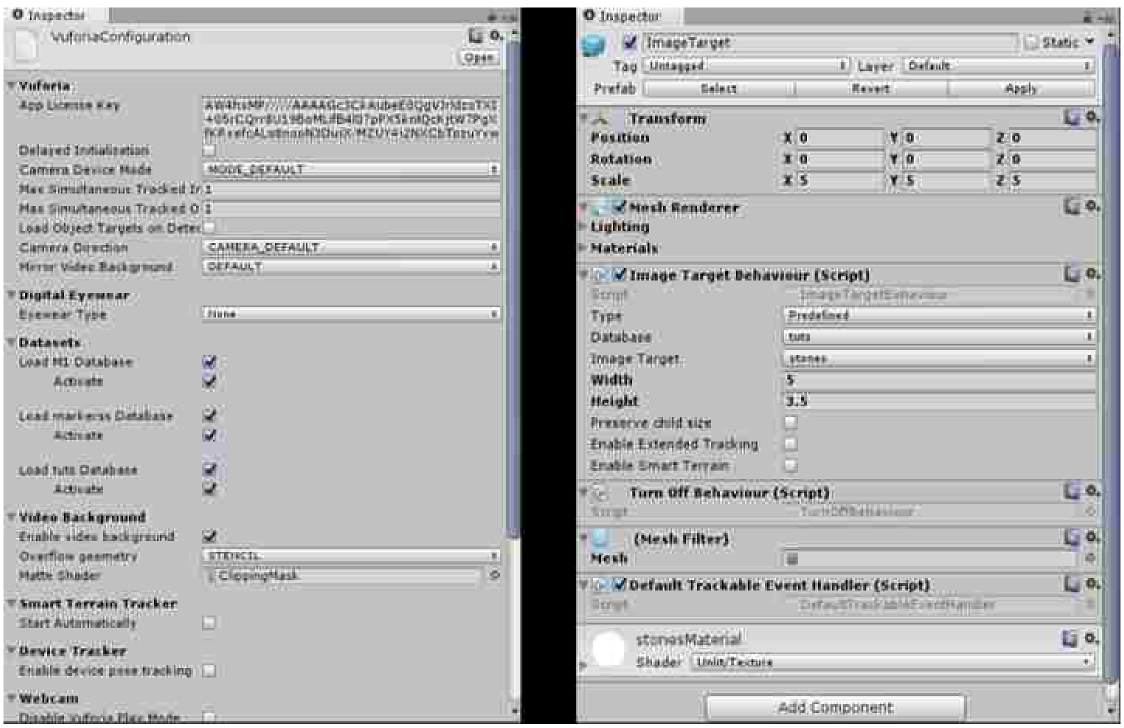

(a) (b)

Figure A.6. (a) The ARCamera prefab (b) The ImageTarget prefab

3. USER DATAGRAM PROTOCOL (UDP) SOCKET

To connect AR system with deep learning network for system implementation, a User Datagram Protocol (UDP) socket is selected for fast speed data transmission for its characteristics of low-latency and low bandwidth. For the system connection, the UDP can be developed by scripting a sender and a receiver for two ends based on the IP address and designated port which is shown in Figure A.8.

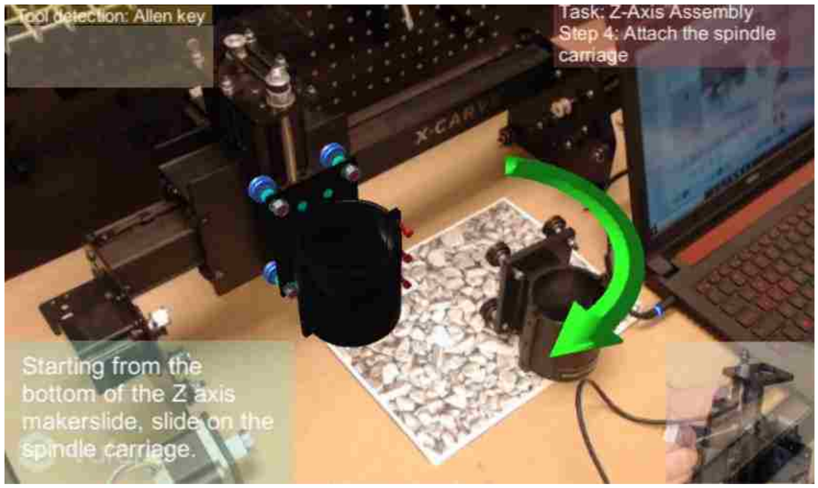

Figure A.7. Unity3D with CAD models augmented for the instruction

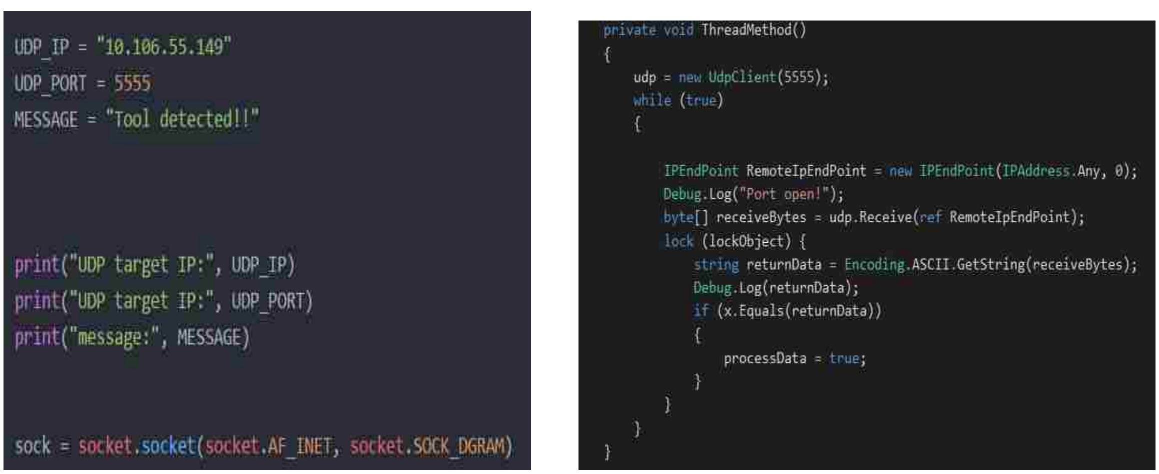

(a) (b)

Figure A.8. (a) The sender scripted in Python (b) The receiver scripted in C#

BIBLIOGRAPHY

[1] https://www.honeywell.com/newsroom/news/2018/02/how-ar-and-vr-are revolutionizing-job-training

[2] https: //runwaygirlnetwork.com/2017/05/17/air-lease-corp-very-disturbed-with-airbus-and-pratt-whitney/

[3] https://www.ge.com/reports/smart-specs-ok-glass-fix-jet-engine/

[4] Hu, Liwen, Ngoc-Tu Nguyen, Wenjin Tao, Ming C. Leu, Xiaoqing Frank Liu, Md Rakib Shahriar, and SM Nahian Al Sunny. "Modeling of Cloud-Based Digital Twins for Smart Manufacturing with MT Connect." Procedia Manufacturing 26 (2018): 1193-1203.

[5] Leu, Ming C., Wenjin Tao, Qiang Niu, and Xiaoyi Chi. "Virtual Bone Surgery." Bio-Materials and Prototyping Applications in Medicine, Second Edition (2018).

[6] Tao, Wenjin, Ze-Hao Lai, and Ming C. Leu. "Manufacturing Assembly Simulations in Virtual and Augmented Reality." Augmented, Virtual, and Mixed Reality Applications in Advanced Manufacturing (2018).

[7] Caudell, Thomas P., and David W. Mizell. "Augmented reality: An application of heads-up display technology to manual manufacturing processes." In *System Sciences, .1992. Proceedings of the Twenty-Fifth Hawaii International Conference on*, vol. 2, pp. 659-669. IEEE, 1992.

[8] Azuma, Ronald T. "A survey of augmented reality." *Presence: Teleoperators & Virtual Environments* 6, no. 4 (1997): 355-385.

[9] Tang, Arthur, Charles Owen, Frank Biocca, and Weimin Mou. "Comparative effectiveness of augmented reality in object assembly." In *Proceedings of the SIGCHI conference on Human factors in computing systems*, pp. 73-80. ACM, 2003.

[10] Khuong, Bui Minh, Kiyoshi Kiyokawa, Andrew Miller, Joseph J. La Viola, Tomohiro Mashita, and Haruo Takemura. "The effectiveness of an AR-based context-aware assembly support system in object assembly." In *Virtual Reality (VR), 2014 iEEE*, pp. 57-62. IEEE, 2014.

[11] Syberfeldt, Anna, Oscar Danielsson, Magnus Holm, and Lihui Wang. "Visual assembling guidance using augmented reality." *Procedia Manufacturing* 1 (2015): 98-109.

[12] Sanna, Andrea, Federico Manuri, Fabrizio Lamberti, Gianluca Paravati, and P. Pezzolla. "Using handheld devices to support augmented reality-based maintenance and assembly tasks." In *Consumer Electronics (ICCE), 2015 IEEE International Conference on*, pp. 178-179. IEEE, 2015.

[13] Dalle Mura, Michela, Gino Dini, and Franco Failli. "An integrated environment based on augmented reality and sensing device for manual assembly workstation *Procedia CIRP* 41 (2016): 340-345.

[14] Webel, Sabine, Uli Bockholt, Timo Engelke, Nirit Gavish, Manuel Olbrich, and Carsten Preusche. "An augmented reality training platform for assembly and maintenance skills." *Robotics and Autonomous Systems* 61, no. 4 (2013): 398-403.

[15] Leu, Ming C., Hoda A. ElMaraghy, Andrew YC Nee, Soh Khim Ong, Michele Lanzetta, Matthias Putz, Wenjuan Zhu, and Alain Bernard. "CAD model based virtual assembly simulation, planning and training." *CIRP Annals* 62, no. 2 (2013): 799-822.

[16] Wu, Shuang, Wenjin Tao, Ming C. Leu, and Suzanna Long. "Engine Sound Simulation and Generation in Driving Simulator." *IISE Annual Conference and Expo 2018, pp. 611-616.*

[17] Werrlich, S., E. Eichstetter, K. Nitsche, and G. Notni. "An Overview of Evaluations Using Augmented Reality for Assembly Training Tasks." *World Academy of Science, Engineering and Technology, International Journal of Computer, Electrical, Automation, Control and Information Engineering* 11, no. 10 (2017): 1074-1080.

[18] Werrlich, Stefan, Kai Nitsche, and Gunther Notni. "Demand Analysis for an Augmented Reality based Assembly Training." In *Proceedings of the 10th International Conference on PErvasive Technologies Related to Assistive Environments*, pp. 416-422. ACM, 2017.

[19] Tao, Wenjin, Ming C. Leu, and Zhaozheng Yin. "American Sign Language alphabet recognition using Convolutional Neural Networks with multiview augmentation and inference fusion." Engineering Applications of Artificial Intelligence 76 (2018): 202-213.

[20] Tao, Wenjin, Ze-Hao Lai, Ming C. Leu, and Zhaozheng Yin. "American Sign Language Alphabet Recognition Using Leap Motion Controller." *IISE Annual Conference and Expo 2018, pp. 599-604.*

[21] Anguita, Davide, Alessandro Ghio, Luca Oneto, Xavier Parra, and Jorge Luis Reyes-Ortiz. "A Public Domain Dataset for Human Activity Recognition using Smartphones." In *ESANN*. 2013.

[22] Anguita, Davide, Alessandro Ghio, Luca Oneto, Francesc Xavier Llanas Parra, and Jorge Luis Reyes Ortiz. "Energy efficient smartphone-based activity recognition using fixed-point arithmetic." *Journal of universal computer science* 19, no. 9 (2013): 1295-1314.

[23] Ward, Jamie A., Paul Lukowicz, Gerhard Troster, and Thad E. Starner. "Activity recognition of assembly tasks using body-worn microphones and accelerometers." *IEEE transactions on pattern analysis and machine intelligence* 28, no. 10 (2006): 1553-1567.

[24] Tao, Wenjin, Ze-Hao Lai, Ming C. Leu, and Zhaozheng Yin. "Worker Activity Recognition in Smart Manufacturing Using IMU and sEMG Signals with Convolutional Neural Networks." Procedia Manufacturing 26 (2018): 1159-1166.

[25] Al-Amin, Md, Wenjin Tao, Ruwen Qin, and Ming C. Leu. "Sensor Data Based Models for Workforce Management in Smart Manufacturing." IISE Annual Conference and Expo 2018, pp. 1955-1960.

[26] LeCun, Yann, Yoshua Bengio, and Geoffrey Hinton. "Deep learning." *nature* 521, no. 7553 (2015): 436.

[27] Krizhevsky, Alex, Ilya Sutskever, and Geoffrey E. Hinton. "Imagenet classification with deep convolutional neural networks." In *Advances in neural information processing systems*, pp. 1097-1105. 2012.

[28] Girshick, Ross, Jeff Donahue, Trevor Darrell, and Jitendra Malik. "Rich feature hierarchies for accurate object detection and semantic segmentation." In *Proceedings of the IEEE conference on computer vision and pattern recognition*, pp. 580-587. 2014.

[29] Girshick, Ross. "Fast r-cnn." *arXiv preprint arXiv:1504.08083*(2015).

[30] Hattori, Hironori, Vishnu Naresh Boddeti, Kris Kitani, and Takeo Kanade. "Learning scene-specific pedestrian detectors without real data." In *Computer Vision and Pattern Recognition (CVPR), 2015 IEEE Conference on*, pp. 3819-3827. IEE 2015.

[31] Peng, Xingchao, Baochen Sun, Karim Ali, and Kate Saenko. "Learning deep object detectors from 3d models." In *Computer Vision (ICCV), 2015 IEEE International Conference on*, pp. 1278-1286. IEEE, 2015.

[32] Ren, Shaoqing, Kaiming He, Ross Girshick, and Jian Sun. "Faster r-cnn: Towards real-time object detection with region proposal networks." In *Advances in neural information processing systems*, pp. 91-99. 2015.

[33] Everingham, Mark, Luc Van Gool, Christopher KI Williams, John Winn, and Andrew Zisserman. "The pascal visual object classes (voc) challenge." *International journal of computer vision* 88, no. 2 (2010): 303-338.

[34] Uijlings, Jasper RR, Koen EA Van De Sande, Theo Gevers, and Arnold WM Smeulders. "Selective search for object recognition." *International journal of computer vision* 104, no. 2 (2013): 154-171.

[35] Huang, Jonathan, Vivek Rathod, Chen Sun, Menglong Zhu, Anoop Korattikara, Alireza Fathi, Ian Fischer et al. "Speed/accuracy trade-offs for modern convolutional object detectors." In *IEEE CVPR*, vol. 4. 2017.

[36] http://x-carve-instructions.inventables.com/750mm/

[37] Hou, Lei, Xiangyu Wang, Leonhard Bernold, and Peter ED Love. "Using animated augmented reality to cognitively guide assembly." *Journal of Computing in Civil Engineering* 27, no. 5 (2013): 439-451.

[38] Leu, Ming C., Wenjin Tao, Amir Ghazanfari, and Krishna Kolan. "NX 12 for Engineering Design." Missouri University of Science and Technology (2017).

VITA

The author of the thesis, Ze-Hao Lai was born in 1991. He received his Bachelor of Science degree in Bio-industrial Mechatronics Engineering from National Chung Hsing University in Taichung City, Taiwan in July 2015. He started pursuing the study for the Master of Science program of Manufacturing Engineering in the Department of Mechanical and Aerospace Engineering at Missouri University of Science and Technology, Rolla, Missouri in August 2016. He received the Master of Science degree in Manufacturing Engineering at Missouri University of Science and Technology in December 2018.